Am J Transl Res 2020;12(3):758-772
www.ajtr.org /ISSN:1943-8141/AJTR0103247

Original Article

LncRNA TUG1 regulates autophagy-mediated endothelial-mesenchymal transition of liver sinusoidal endothelial cells by sponging miR-142-3p

Rui Zhang[1*], Xiao-Quan Huang[1*], Ying-Yi Jiang[1*], Na Li[2], Jian Wang[1], Shi-Yao Chen[1,3,4]

Departments of [1]Gastroenterology and Hepatology, [2]Infectious Diseases, [3]Endoscopy Center and Endoscopy Research Institute, Zhongshan Hospital, Fudan University, Shanghai, P. R. China; [4]Shanghai Institute of Liver Disease, Shanghai, P. R. China. [*]Equal contributors.

Received October 8, 2019; Accepted February 20, 2020; Epub March 15, 2020; Published March 30, 2020

Abstract: Accumulating evidence indicates that competing endogenous RNA networks play a critical role in cirrhosis progression. However, their biological role and regulatory mechanisms in liver sinusoidal endothelial cells (LSECs) have not been explored. Here, we exposed LSECs to starvation and lipopolysaccharide (LPS) treatment and assessed changes in TUG1 and miR-142-3p expression, autophagy, and endothelial-mesenchymal transition (EndMT). We confirmed the effects of targeted binding between miR-142-3p and TUG1 or ATG5 by luciferase activity and radio-immunoprecipitation assay. Using an *in vivo* rat model of cirrhosis, we evaluated autophagy and EndMT in LSECs by immunofluorescence co-localization and immunohistochemical staining. The diagnostic efficiency of miR-142-3p and LPS were determined by receiver-operating characteristic curve analysis. We found that LSECs survived starvation by activating autophagy. LPS treatment enhanced autophagy and promoted EndMT of LSECs by upregulating TUG1. Our rat model of cirrhosis confirmed that serum LPS level, autophagy, and EndMT were increased in LSECs. TUG1 was highly expressed in LSECs, and TUG1 knockdown suppressed ATG5-mediated autophagy and EndMT of LSECs. TUG1 regulated ATG5 via shared miR-142-3p response elements. miR-142-3p was expressed at low levels in LSECs and negatively regulated autophagy and EndMT by reducing ATG5 expression. Our results suggest that TUG1 promotes LPS-induced autophagy and EndMT of LSECs by functioning as an endogenous sponge for miR-142-3p and promoting the expression of ATG5. LPS and miR-142-3p are potential diagnostic and therapeutic targets in cirrhosis.

Keywords: Autophagy, endothelial-mesenchymal transition, liver sinusoidal endothelial cells, miR-142-3p, TUG1

Introduction

A late manifestation of various chronic liver diseases, liver cirrhosis is characterized by a hypercoagulative state and changes in intestinal mucosal permeability, which often signify sinusoidal microthrombotic events and increased bacterial translocation. This often causes micro-infarcts/ischemia and gram-negative bacterial endotoxin (i.e., lipopolysaccharide, LPS) elevation [1-4], leading to tissue collapse and additional microcirculatory dysfunction and contributing to fibrosis progression and increased risk of death or poor prognosis [5-7]. Hepatic sinusoids support an efficient network of liver parenchyma and are strongly implicated in the pathogenesis of liver cirrhosis. Liver sinusoidal endothelial cells (LSECs) make up ~20% of cells in hepatic sinusoids and play a crucial role in the hemodynamics of sinusoidal microcirculation [8, 9]. Pathophysiological abnormalities can have serious adverse effects on LSECs. In turn, damaged LSECs can initiate fibrosis development through alterations of their morphology and function [10-12]. Therefore, targeting LSECs has great therapeutic potential for liver diseases. However, how LSECs adapt to microvascular infarcts/ischemia and high environmental concentrations of LPS is not known.

Autophagy is a cell-conserved process that maintains cellular homeostasis in response to diverse extracellular stresses that influence cell fate [13]. Autophagy is implicated in liver fibro-

sis and cirrhosis [14-17]. Although previous studies show increased autophagy of LSECs in the human fibrotic liver [18], they did not explore how LSEC autophagy initiates liver cirrhosis. In addition, endothelial-mesenchymal transition (EndMT) is a dynamic process whereby endothelial cells acquire myofibroblastic features, characterized by a loss of cell-cell junctions and endothelial markers and a gain of mesenchymal cell markers. As accumulating evidence points to the importance of EndMT in various forms of fibrosis progression [19-21], we hypothesize that LSECs promote cirrhosis progression through their autophagy-mediated EndMT.

Long noncoding RNAs (lncRNAs) are 200 nucleotide (nt)-long transcripts that function as competing endogenous RNAs (ceRNAs) that compete for microRNA (miRNA) binding, thereby derepressing the expression of miRNA-targeted mRNAs and altering their response to various stimuli at transcriptional and posttranscriptional levels. lncRNA taurine-upregulated gene 1 (TUG1) is a 7.6-kb gene located at chr22q12.2 that is named for its upregulation by taurine treatment [22]. Aberrant TUG1 is observed in several biological processes (e.g., cell proliferation, apoptosis, EndMT) and disorders (e.g., tumor initiation, liver fibrosis, myocardial fibrosis) [23-26].

Here, we investigated the role of a ceRNA network consisting of TUG1, miR-142-3p, and autophagy-related 5 (ATG5) in the autophagy and EndMT of LSECs under starvation (an ischemic condition [27]) and exposed to high environmental levels of LPS as an *in vitro* model of liver cirrhosis.

Materials and methods

Cell line, cell culture and cell treatment

Primary human LSECs were routinely maintained in complete endothelial cell medium (ECM) containing 5% heat-inactivated fetal bovine serum (FBS), 1% endothelial growth supplement, and 1% penicillin/streptomycin (all acquired from Sciencell, CA, USA). Cells were incubated in a humidified chamber with a 5% CO_2 atmosphere at 37°C. For the starvation condition, LSECs were cultured in ECM without FBS.

Cell proliferation and cell cycle assays

Cell proliferation was determined using WST-1 assay. Briefly, 1×10^4 cells were seeded into 96-well plates in triplicate under routine or starvation conditions for 8, 16, or 24 h. Optical density was measured by absorbance at 450 nm.

Cell cycle analysis was conducted using flow cytometry. After culturing under routine or starvation conditions for 24 h, cells were harvested, washed, fixed, and incubated with PI/RNase staining buffer (BD Biosciences, MD, USA) for 15 min at room temperature.

Transwell assay

LSECs transfected with negative control (NC) mimic, miR-142-3p mimics, smart silencer NC, TUG1 smart silencer, short hairpin RNA (shRNA) against ATG5, or corresponding negative lentiviral vector control were cultured under normal, starvation, or starvation plus 1 μg/mL LPS conditions. Migration ability was evaluated using 24-well plates (Corning Costar, MA, USA) with 8-μm pore size (Millipore, MA, USA). Approximately 5×10^4 cells in 200 μL FBS-free ECM were added to the upper chamber of each well, and 600 μL complete ECM was placed in the bottom chamber. After 12 h incubation, migrated cells were fixed in methanol, stained with crystal violet, and counted in three random fields using a phase-contrast microscope (Olympus, Tokyo, Japan).

Cell transfection in vitro

NC mimic, miR-142-3p mimics, smart silencer NC, TUG1 smart silencer, and riboFECT CP transfection kits were acquired from RiboBio (Guangzhou, China). Transfection of all aforementioned RNA reagents at a final concentration of 100 nM was performed in accordance with the manufacturer's instructions.

Lentiviral vectors expressing shRNA against ATG5 and corresponding negative lentiviral vector control were purchased from Genechem (Shanghai, China). Human LSECs were transduced with a 10 multiplicity of infection of lentivirus. The stability of shRNA transfection in ATG5 cell lines was validated using western blot analysis.

Autophagy analysis

Tandem fluorescence-tagged LV6-mCherry-GFP-LC3B lentiviral vector (GenePharma, Shanghai, China) transduction and electron microscopy were used to detect autophagy. mCherry fluorescence was relatively stable under the acidic conditions of the lysosome lumen, whereas green fluorescence protein (GFP) was sensitive to this acidic condition. Transfection with the LV6-mCherry-GFP-LC3B lentiviral vector revealed the formation of autophagosomes that were not fused with lysosomes in human LSECs. Representative images with identical parameter settings were captured using a confocal microscope (Olympus BX51).

Structural analysis of autophagy as visualized by accumulation of double-membraned cytoplasmic vesicles was performed by transmission electron microscopy (TEM). Cells were harvested and fixed with a mixture of 2.5% glutaraldehyde and 0.1 mol/L sodium cacodylate at 4°C overnight. Specimens were then dehydrated using ethanol and propylene oxide, embedded in Araldite, cut into ultra-thin sections (50-60 nm), and stained with 3% lead citrate-uranyl acetate. Images were obtained using a JEM-1200 electron microscope (JEOL, Tokyo, Japan).

Quantitative real-time reverse transcriptase-polymerase chain reaction (qRT-PCR) and miRcute plus miRNA qRT-PCR

Total RNA was extracted from human LSECs using TRIzol reagent (Ambion, CA, USA). According to the manufacturer's instructions, complementary DNA (cDNA) was synthesized and amplified using the RevertAid First-Strand cDNA Synthesis Kit and Maxima SYBR Green qPCR Master Mix Kit (Thermo Fisher Scientific, MA, USA). Primers for TUG1, metastasis-associated lung adenocarcinoma transcript 1 (MALAT1), nuclear paraspeckle assembly transcript 1 (NEAT1), maternally expressed 3 (MEG3), small nucleolar RNA host gene 5 (SNHG5), miR-142-3p, and U6 were acquired from RiboBio. Relative gene expression was normalized to that of internal control (glyceraldehyde-3-phosphate dehydrogenase (GAPDH) for mRNA and lncRNA, U6 for miRNA) using the $2^{-\Delta\Delta Ct}$ method.

This study was approved by the Clinical Research Ethics Committee of Zhongshan Hospital. From September 2017 to May 2018, serum samples were obtained from patients pathologically diagnosed with liver cirrhosis and healthy control volunteers. All participants signed informed consent forms permitting the use of serum samples and clinical profiles for research. Extraction of serum miRNA was performed using the miRcute Serum/Plasma miRNA Isolation Kit (Tiangen, Beijing, China) following the manufacturer's instructions. For miRNA analysis, cDNA synthesis and qRT-PCR analysis were performed using the miRcute miRNA First-Strand cDNA Synthesis Kit and miRcute miRNA qPCR Detection Kit (Tiangen, Beijing, China). The expression of miRNAs in serum samples was normalized to that of external control (Tiangen) as a reference. The primer sequences of target genes are presented in Table S1.

Co-immunofluorescence staining

Samples were fixed with 4% paraformaldehyde at room temperature for 10 min, permeabilized with 0.1% Triton X-100 (Sangon Biotech, China), and blocked with 1% bovine serum albumin in phosphate-buffered saline (PBS). Slides were then co-incubated with α-SMA (1:100, Boster) or LC3B (1:100, Cell Signaling Technology) and CD31 (1:2,000, Abcam) overnight at 4°C. Slides were then incubated with secondary antibodies conjugated to Alexa Fluor 488/594 (1:400, Life Technologies) along with DAPI (Roche, Mannheim, Germany) in the dark. Immunofluorescence images were captured by a fluorescence microscope (Olympus BX51).

Immunohistochemical staining analysis

Paraffin-fixed tissues from healthy control rats and those with liver cirrhosis were deparaffinized and rehydrated. After blocking with goat serum, slides were probed with primary antibodies against vimentin (1:100, Boster), α-SMA (1:100, Boster), LC3B (1:100, Proteintech), or CD31 (1:2,000, Abcam) at 4°C overnight and then incubated with secondary antibodies. Sections were visualized using 3,3'-diaminobenzidine solution and observed under a light microscope at 200 × magnification.

Western blot analysis

Total protein was lysed and extracted using radio-immunoprecipitation assay buffer (Beyo-

time Biotechnology, China) supplemented with 1 mM PMSF and 1 mg/mL phosphatase inhibitors (Roche). Following protein quantification using the Bicinchoninic Acid Protein Assay Kit (Thermo Scientific), equal amounts of samples were loaded onto sodium dodecyl sulfate-polyacrylamide gel (SDS-PAGE) for separation and electrotransferred to polyvinylidene difluoride membranes (Millipore). After blocking with 5% non-fat milk and incubating with primary antibodies, membranes were incubated with secondary antibodies (Table S2). Chemiluminescence reagents (Millipore) were used to detect bands with specific immune complexes.

RNA sequencing (RNA-seq) analysis

Primary human LSECs were collected and lysed with TRIzol reagent. The RNA-seq library was constructed using the TruSeq Stranded Total RNA Library Prep Kit (Illumina) according to supplied protocols [28]. Briefly, after rRNA depletion, cDNA synthesis, and poly(A) addition, the cDNA library was amplified, and small RNA-seq libraries were built. Gene expression was calculated based on Fragments per Kilobase per Million Mapped Fragments. Due to the high expression of endothelial coding genes (i.e., vascular endothelial growth factor A [VEGFA]) in human LSECs, lncRNAs with well-conserved sequences between species and expression levels higher than that of VEGFA were screened and validated [28].

Luciferase reporter assay

pGL3 promoter-hTUG1 wild type (WT) or pGL3 promoter-hATG5 WT with a potential miR-142-3p-binding site or mutation (MUT) site was synthesized and constructed by Genechem (Shanghai, China) (Table S3). Briefly, HEK293T cells were co-transfected with 1 μg pATG5-miR-142-3p-UTR-WT or pATG5-miR-142-3p-UTR-MUT and pTUG1-miR-142-3p-UTR-WT or pTUG1-miR-142-3pUTR-MUT with 100 nM Lipofectamine 2000 reagent (Invitrogen, CA, USA). Approximately 48 h after transfection, luciferase assay was performed using the Dual-Luciferase Reporter Assay System (Promega, WI, USA) according to the manufacturer's instructions. Firefly luciferase activity was normalized to Renilla luciferase activity. Each experiment was performed in triplicate.

Fluorescence in situ hybridization (FISH)

FISH (RiboBio) was conducted on LSECs according to the manufacturer's instructions. Briefly, LSECs were rinsed in cold PBS, fixed with 4% formaldehyde, and permeabilized using 0.5% Triton X-100 for 5 min. After blocking with prehybridization buffer at 37°C for 30 min, hybridization was performed with lncRNA-TUG1, 18S, or U6 FISH probe at 37°C overnight. Cells were then washed with saline sodium citrate buffer (Sangon Biotech) followed by cell nuclei counterstaining using DAPI (Roche). Images were captured using a confocal microscope.

RNA binding protein immunoprecipitation assay

RNA immunoprecipitation (RIP) experiments were carried out using the RNA Immunoprecipitation Kit (Sigma, USA) in accordance with the manufacturer's instructions. Briefly, LSECs (~10^7) were lysed on ice and incubated with 100 μL RIP wash buffer containing magnetic beads conjugated to human anti-Argonaute 2 (anti-Ago2) antibody (Abcam) or immunoglobulin G (IgG) control. The retrieved RNA fraction was subjected to qRT-PCR to measure the expression of TUG1, miR-142-3p, and ATG5. The primers used for detecting TUG1, miR-142-3p, ATG5, U6, and GAPDH are listed in Table S4.

Enzyme-linked immunosorbent assay (ELISA)

Concentrations of LPS in the serum of rats and patients were determined using rat and human LPS ELISA Kits (NEWGEORGE, China) in accordance with the manufacturer's instructions. Each sample was performed with three replicates, and three independent experiments were carried out.

Animals

Experimental protocols involving animals were approved by the Animal Care and Use Committee of Fudan University and Zhongshan Hospital Research Ethics Committee (Shanghai, China). Briefly, a liver cirrhosis model was established using male Sprague-Dawley rats (weighing ~200 g; Shanghai Laboratory Animal Research Center) receiving an intraperitoneal injection of CCl4 (Sigma; diluted 1:1 in olive oil, 1.5 mL/kg) twice a week for 5 weeks (n = 4).

Control rats (n = 4) were intraperitoneally injected with vehicle (1.5 mL/kg olive oil) at the same time intervals. Thereafter, serum was collected for LPS detection, and liver samples were harvested for immunohistochemical staining.

Statistical analysis

All data are expressed as mean ± standard deviation. Comparisons between two groups or among more than two groups were performed by Student's *t*-tests or one-way ANOVA, respectively, using GraphPad Prism software (San Diego, CA, USA). Receiver-operating characteristic (ROC) curve analysis was used to determine the diagnostic efficiency of the parameters, and differences in the area under the curve (AUC) were detected using SPSS 24.0 (IL, USA). A *P*-value < 0.05 was considered statistically significant.

Results

Starvation promoted activation of autophagy in LSECs

To examine the effects of starvation conditions in cirrhosis, we cultured LSECs in starvation medium, which resulted in a stagnant growth state without obvious proliferation (**Figure 1A**). Consistently, an increased proportion of starved LSECs were in G0/G1 phase of the cell cycle, indicating their slow growth state (**Figure 1B**). To determine whether LSECs survive starvation via autophagy, we analyzed changes in autophagy-associated gene expression in starved LSECs. RT-PCR and western blotting revealed that LC3B, ATG5, ATG7, and Beclin1 expression were significantly upregulated, whereas P62 expression was significantly downregulated (**Figure 1C**). The expression of LC3B and P62 were further increased after exposure to chloroquine (CQ) as evidenced by western blot analysis (**Figures 1D** and S1). Next, we stably transfected LSECs with mCherry-GFP-LC3 lentivirus to directly visualize the presence of autophagic flux. As shown in **Figure 1E**, starvation enhanced the accumulation of red dots in LSECs. Consistent with this finding, we detected double-membraned cytoplasmic vesicles by TEM, which confirmed the occurrence of autophagy in LSECs (**Figure 1F**). These results suggest that starvation stimulation promotes autophagy in LSECs.

LPS promoted EndMT of LSECs by increasing autophagy

We observed elevated serum LPS levels as detected by ELISA in an established rat models of cirrhosis (**Figure 2A**). We also observed increased autophagy and EndMT of LSECs in cirrhotic liver samples as evidenced by increased expression of LC3B, α-SMA, and vimentin and decreased expression of CD31 via immunofluorescence and immunohistochemical staining (**Figures 2B** and S2). Thus, we investigated whether increased autophagy is responsible for the EndMT of LSECs after LPS treatment *in vitro*. As shown in **Figure 3A**, LPS treatment further increased starvation-induced autophagy by upregulating expression of autophagy-associated genes LC3B and ATG5 and downregulating expression of P62. LPS treatment also increased EndMT of LSECs as evidenced by increased expression of α-SMA and decreased expression of VE-cadherin and CD31 in a dose- and time-dependent manner (**Figures 3B-D** and S3). The (dose-dependent) increase of autophagy-related gene expression of ATG7 and Beclin1 by LPS in LSECs were not as prominent as ATG5 and therefore ATG5 was selected as the targeted gene of autophagy (**Figures 3B** and S3). Knockdown of ATG5 decreased LSEC migration ability, autophagy and EndMT by downregulating LC3B, and α-SMA expression and upregulating P62, CD31, and VE-cadherin expression (**Figures 3E**, **3F** and S3), which was partially reversed by LPS treatment. These findings indicate that LPS increases EndMT of LSECs by promoting autophagy.

TUG1 promoted LPS-mediated autophagy and EndMT of LSECs

To identify the main mediator of LPS-promoted autophagy and EndMT of LSECs, we performed deep sequencing of poly(A)-selected RNA isolated from LSECs. We found that 42.12% of total RNA was noncoding RNAs (ncRNA), of which 10.84% were intragenic natural antisense transcripts, 10.22% were long intergenic ncRNAs, and 21.05% were other ncRNAs (**Figure 4A**). By filtering data by lncRNA annotation and expression levels, we identified transcripts with expression levels comparable to that of the endothelial coding gene VEGFA. As shown in **Figure 4B**, we selected five highly expressed lncRNAs (MALAT1, NEAT1, MEG3,

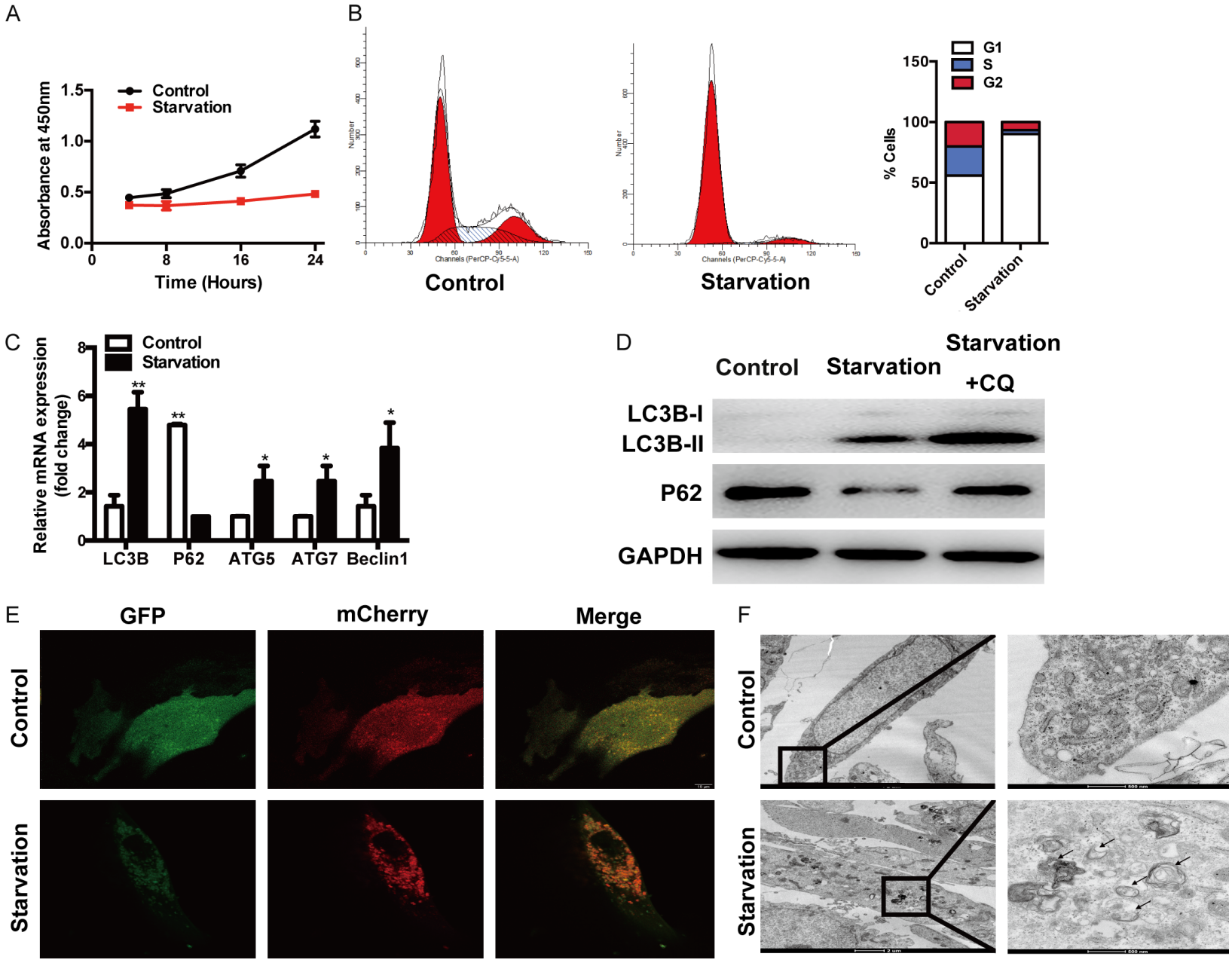
A
Absorbance at 450nm
Control
Starvation
Time (Hours)
B
Control
Starvation
G1
S
G2
% Cells
C
Relative mRNA expression (fold change)
LC3B
P62
ATG5
ATG7
Beclin1
D
Control
Starvation
Starvation +CQ
LC3B-I
LC3B-II
P62
GAPDH
E
GFP
mCherry
Merge
F

Figure 1. Starvation activated autophagy in LSECs. A. WST-1 assay revealed that starvation significantly inhibited LSEC proliferation. B. Flow cytometry showed an increased proportion of LSECs in the G0/G1 phase when cultured under starvation. C. Quantitative RT-PCR showed the expression of autophagy-related genes (LC3B, ATG5, ATG7, Beclin1, and P62) in LSECs under starvation. D. The protein expression of LC3B and P62 in LSECs under starvation and starvation plus CQ conditions was assessed by western blot analysis. E, F. An increase in autophagic flux in LSECs under starvation was validated by punctate mCherry-GFP-LC3 fusion protein expression using confocal microscopy and double-membraned cytoplasmic vesicles (black arrow) using TEM. CQ, 1.5 μM; **, $P < 0.01$; *, $P < 0.05$.

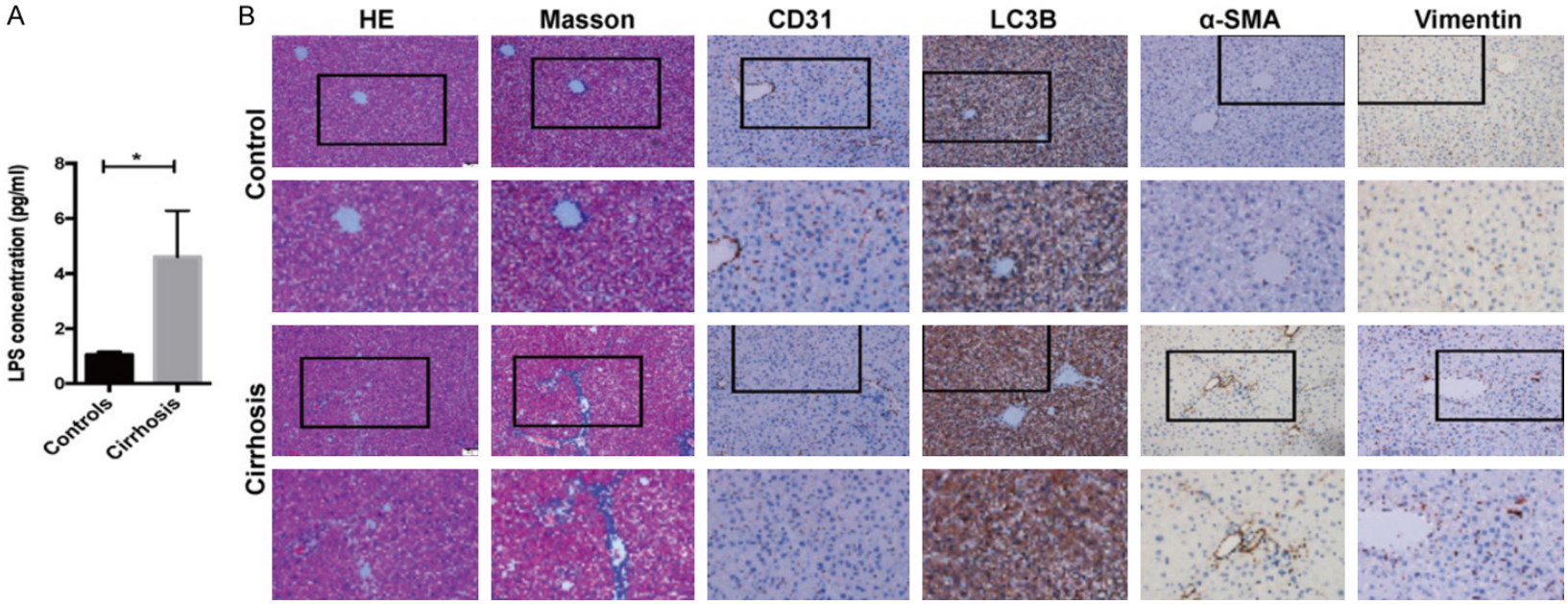

Figure 2. Increased autophagy and EndMT of LSECs in a rat model of cirrhosis. A. Elevated serum LPS levels were detected in cirrhotic rats. B. Pathological changes in CCl4-induced liver cirrhosis were examined by H&E and Masson's trichrome. The expression of autophagy and EndMT proteins (LC3B, CD31, α-SMA, and vimentin) in normal and cirrhotic rats was examined by immunohistochemical staining. **, $P < 0.01$; *, $P < 0.05$.

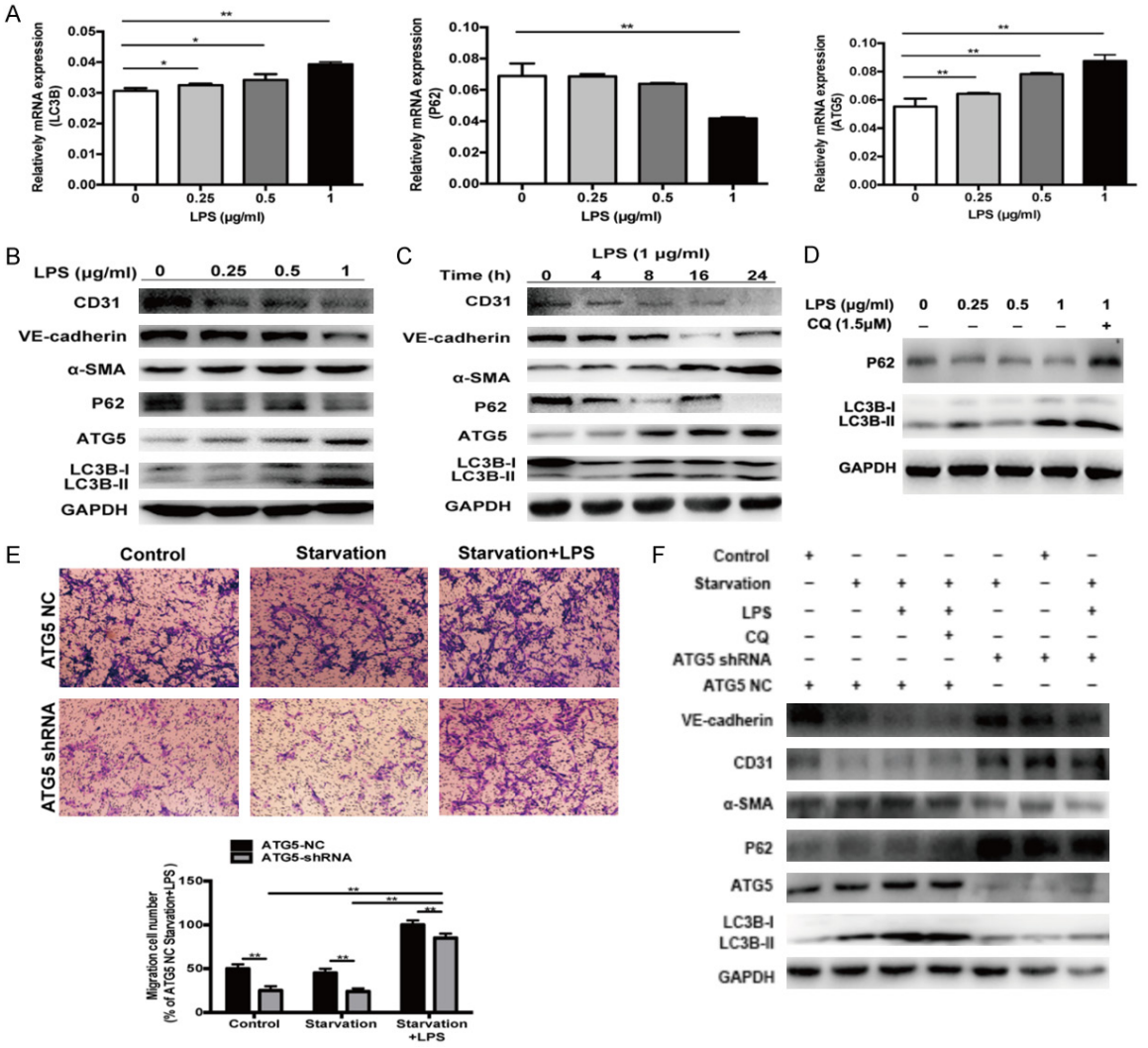

Figure 3. LPS promoted EndMT of LSECs by increasing autophagy. A. As indicated by ectopic expression of LC3B, ATG5, and P62, LPS treatment promoted starvation-induced autophagy in a dose-dependent manner. B, C. Dose- and time-dependent expressions of autophagy (LC3B, ATG5, and p62) and EndMT (α-SMA, VE-cadherin, and CD31) proteins in LSECs under starvation treated with LPS was examined by western blot analysis. D. The increased expression of LC3B and P62 after LPS treatment was further elevated by CQ. E. Transwell assay revealed that ATG5 knockdown suppressed the migration ability of LSECs, which was partially reversed by LPS treatment. F. Knockdown of ATG5 decreased autophagy and EndMT of LSECs as shown by the decreased expressions of LC3B and α-SMA, and increased expressions of P62, CD31, and VE-cadherin. These effects were partially reversed LPS treatment. CQ, 1.5 μM; **, $P < 0.01$; *, $P < 0.05$.

SNHG5, and TUG1) whose sequences are well conserved across species and confirmed their expression by RT-PCR after LPS treatment under starvation. The most profoundly upregulated lncRNA was TUG1, which showed a dose-dependent increase in expression in response to LPS treatment (**Figure 4C**). As TUG1 was more than 7000 nt long and highly expressed in LSECs, we further explored its role in the regulation of autophagy and EndMT of LSECs by silencing its expression. We found that TUG1 knockdown reduced LSEC migration ability; decreased levels of LC3B, ATG5, and α-SMA expression; and increased levels of p62, VE-cadherin, and CD31 expression (**Figures 4D-F** and S4). These effects were partially reversed by LPS treatment. These results show that TUG1 mediates the regulation of autophagy and EndMT of LPS-treated LSECs under starvation.

TUG1 promoted autophagy and EndMT of LSECs by targeting ATG5

As we found shows that starvation and LPS treatment elevated the expression of both

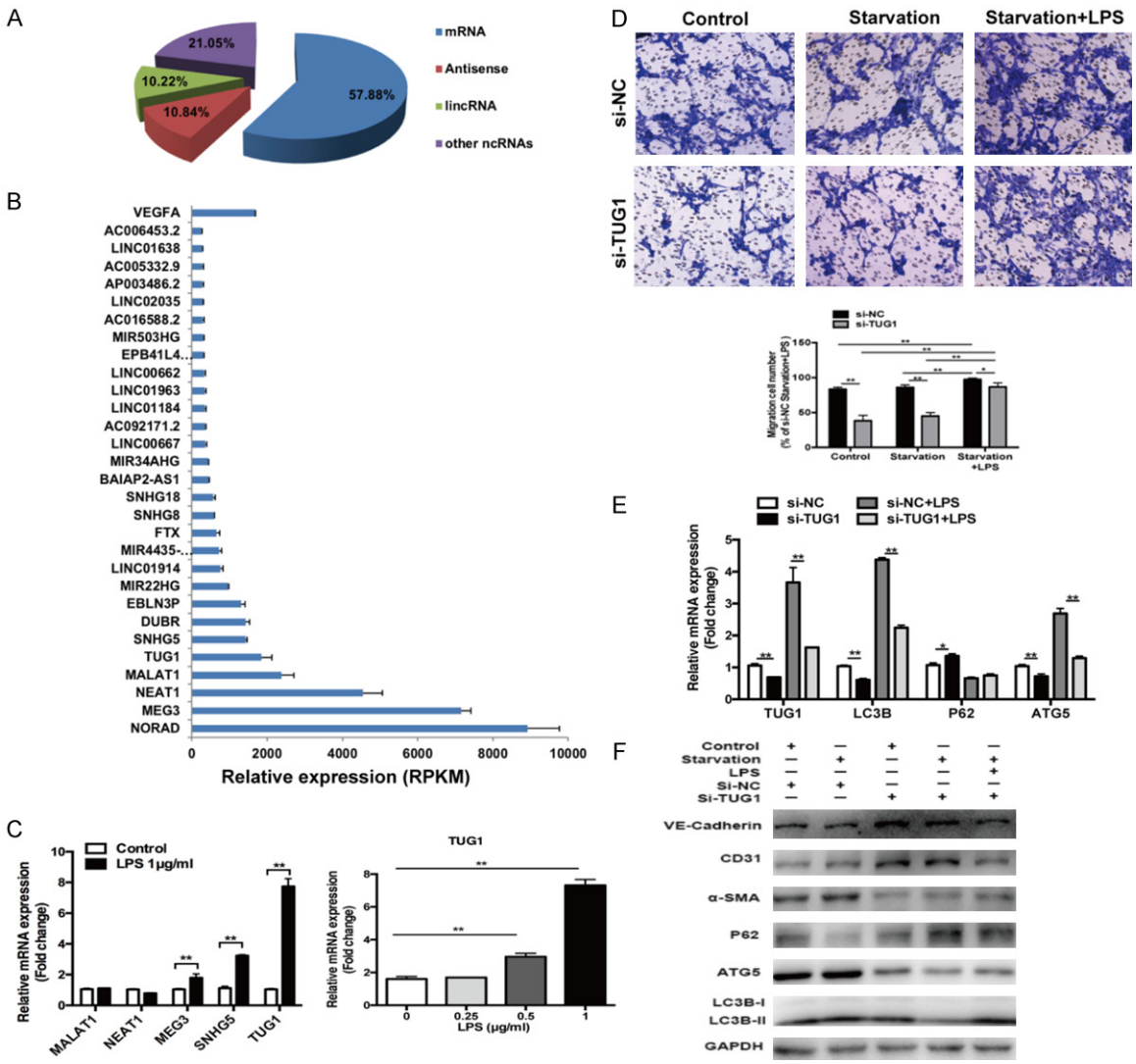

Figure 4. TUG1 promoted LPS-mediated autophagy and EndMT of LSECs. A. Poly(A) RNA of LSECs was detected by deep sequencing. B. Expression levels of lncRNAs comparable with that of VEGFA. C. RT-PCR analysis of five highly expressed lncRNAs (MALAT1, NEAT1, MEG3, SNHG5, and TUG1) in LSECs. TUG1 was most markedly elevated in LPS-treated LSECs and was upregulated in a dose-dependent manner. D. Transwell assay revealed that TUG1 knockdown suppressed the migration ability of LSECs, which was partially reversed by LPS treatment. E, F. TUG1 knockdown suppressed autophagy and EndMT of LSECs as evidenced by the changes in LC3B, ATG5, P62, VE-cadherin, CD31, and α-SMA in LSECs. LPS, 1 μg/ml. **, $P < 0.01$; *, $P < 0.05$.

TUG1 and ATG5 and that ATG5 was upregulated autophagy-related gene in starved LSECs after LPS treatment, we tested whether TUG1 promoted autophagy and EndMT by targeting ATG5. We found that TUG1 knockdown reduced the expression of ATG5 in LSECs, which was also associated with reduced autophagy and EndMT (**Figures 3F**, **4E**, **4F**). These results suggest that ATG5 mediates the effects of TUG1 on autophagy and EndMT of LPS-treated LSECs under starvation.

TUG1 modulated ATG5 through cross-talk with miRNA-142-3p

lncRNAs have regulatory roles as cis- or trans-regulators of gene activity via various mechanisms depending on their location in the nucleus or cytoplasm. If mainly localized in the nucleus, lncRNAs bring together proteins to form ribonucleoprotein complexes by functioning as scaffolds and recruit chromatin-modifying complexes to target genes [29]. If mainly localized

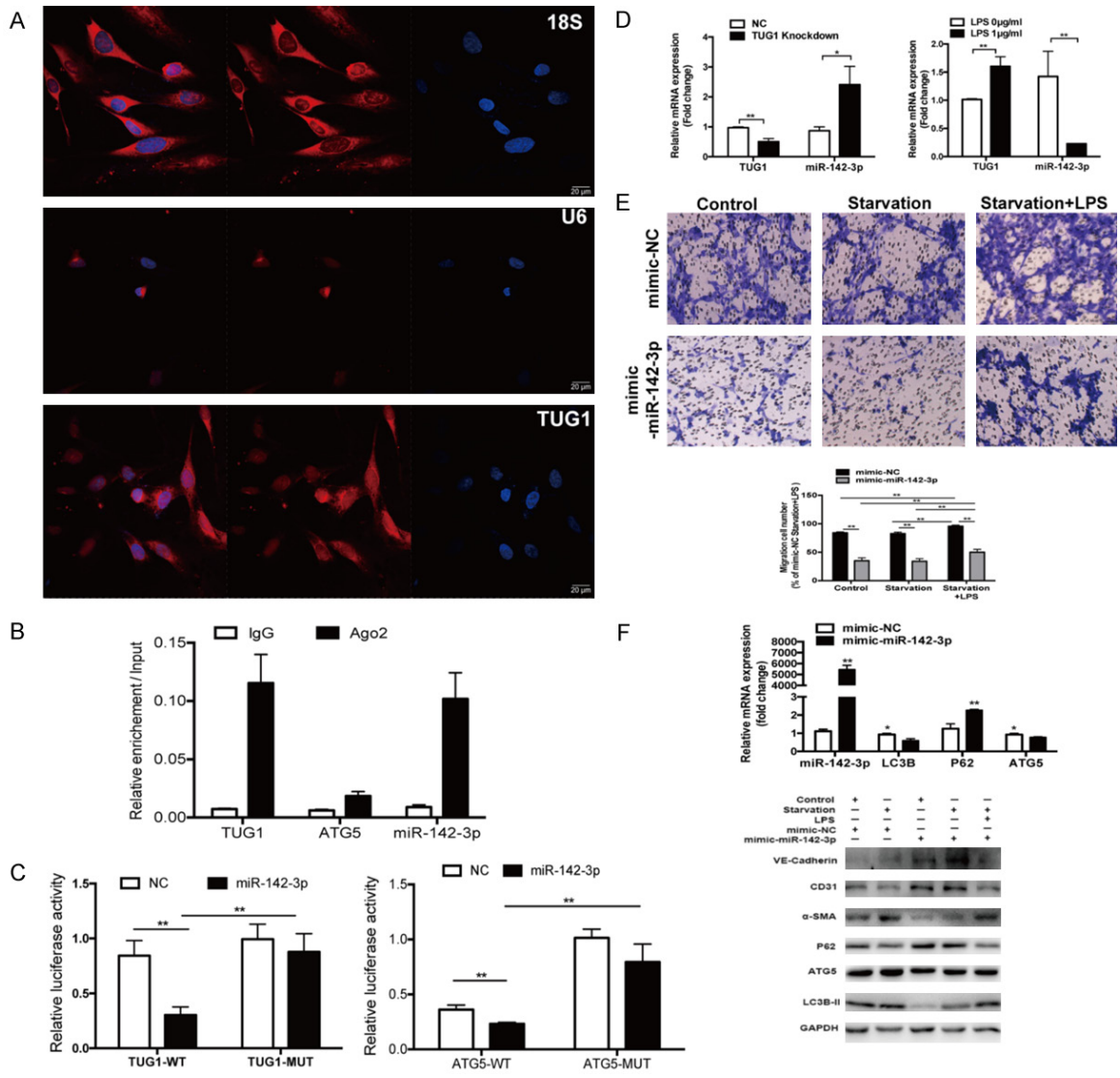

Figure 5. TUG1 modulated ATG5 through cross-talk with miRNA-142-3p. A. RNA FISH assay of TUG1 in LSECs. B. RIP with an antibody against Ago2 in LSECs showed that TUG1, ATG5, and miRNA-142-3p were more preferentially enriched in the anti-Ago2 group than in the anti-normal IgG group. C. Dual-luciferase reporter assay revealed that miR-142-3p-overexpressing plasmid decreased the luciferase activity in the WT vectors of TUG1 and ATG5 compared with that in the MUT vectors. D. Expression of miR-142-3p in LSECs after TUG1 knockdown or LPS-induced overexpression was confirmed by RT-PCR. E, F. Migration ability and changes in LC3B, ATG5, P62, α-SMA, VE-cadherin, and CD31 expression after transfection of miRNA-142-3p mimics in LSECs treated with LPS were analyzed by Transwell assay, RT-PCR, and western blot analysis. LPS, 1 μg/ml. **, $P < 0.01$; *, $P < 0.05$.

in the cytoplasm, they can competitively bind miRNA to modulate the derepression of miRNA targets [30]. RNA FISH assay demonstrated that TUG1 was abundant in both the cytoplasm and nucleus (**Figure 5A**). Thus, we hypothesized that TUG1 regulates the expression of ATG5 by engaging in crosstalk with miRNAs. To test this hypothesis, we performed RIP with an antibody against Ago2 in LSECs. We found that TUG1 and ATG5 were recruited to Ago2-related RNA-induced silencing complexes (RISCs) and may interact with miRNAs, suggesting that miRNAs may play essential roles in TUG1-mediated regulation of ATG5 (**Figure 5B**).

To identify the miRNAs that potentially target TUG1 and ATG5 transcripts, we used StarBase v2.0 (http://starbase.sysu.edu.cn/), which showed that both TUG1 and ATG5 had a putative binding site for miR-142-3p. To confirm

Table 1. The baseline characteristics of recruited two cohorts

Characteristics	Health Controls (n = 20)	Cirrhosis (n = 40)	*p*-value
Age (years) (mean ± SD)	59.25±6.15	57.33±12.58	0.52
Gender (Male/Female)	10/10	20/20	1.00
Etiology			
HBV	-	19 (47.5%)	-
HCV	-	1 (2.5%)	-
Alcohol	-	3 (7.5%)	-
PBC	-	4 (10%)	-
Schistosomiasis	-	4 (10%)	-
Cryptogenic	-	6 (15%)	-
AIH	-	2 (5%)	-
Mixed	-	1 (2.5%)	-
Child-Pugh classification			
Class A	-	24 (60%)	-
Class B	-	14 (35%)	-
Class C	-	2 (5%)	-
Laboratory parameters			
ALT (U/L) (mean ± SD)	20.1±11.13	24.18±10.76	0.18
AST (U/L) (mean ± SD)	17.1±5.34	36.45±13.77	< 0.0001
Prothrombin time (S) (mean ± SD)	10.92±0.83	14.11±2.48	< 0.0001
Albumin (g/L) (mean ± SD)	44.2±2.53	36.98±5.44	< 0.0001
Ascites (Presence/Absent)	0/20	19/21	< 0.0001
Total Bilirubin (μmol/L) (mean ± SD)	10.92±3.88	21.1±13.39	0.0016

HCV, hepatitis C virus; HBV, hepatitis B virus; AIH, autoimmune hepatitis; PBC, primary biliary cirrhosis; ALT, alanine aminotransferase; AST, aspartate aminotransferase.

whether TUG1 and ATG5 are regulated by miR-142-3p, we constructed luciferase reporters with WT or MUT putative binding sites for TUG1 or ATG5. We found that miR-142-3p-overexpressing plasmid decreased the luciferase activity in the WT vectors of TUG1 and ATG5 compared with that in the MUT vectors (**Figure 5C**). Furthermore, RIP showed that TUG1 and miR-142-3p were more enriched in the anti-Ago2 group compared with the anti-normal IgG group, indicating that TUG1 and miR-142-3p were in the same RISC (**Figure 5B**). Next, we confirmed that the expression of miR-142-3p was elevated in LSECs when TUG1 was down-regulated. By contrast, when TUG1 was overexpressed by LPS treatment, the level of miR-142-3p declined (**Figure 5D**). These results imply that TUG1 negatively regulates the expression of miR-142-3p.

miR-142-3p was expressed at low levels in LSECs. To further delineate the biological interaction between miR-142-3p and ATG5, we used RT-PCR and immunoblot to assess ATG5 levels in LSECs after transduction with miR-142-3p mimics. As demonstrated in **Figures 5E**, **5F** and S5, transfection of miRNA-142-3p mimics decreased the migration ability and expression of ATG5 in LSECs. During this process, EndMT and autophagy were also inhibited, as exemplified by decreased expression of LC3B and α-SMA and the increased expression of P62, VE-cadherin, and CD31. These effects were partially reversed by LPS treatment. These findings indicate that ATG5 is a downstream target of miR-142-3p. Moreover, miR-142-3p served as a suppressor of autophagy and EndMT and reversed the effects of starvation and LPS treatment on LSECs.

Taken together, these results indicated that TUG1 may act as a competitive endogenous miR-142-3p sponge and thereby regulate the autophagy-mediated EndMT targeting of ATG5.

Diagnostic performance of serum LPS and miR-142-3p among cirrhosis patients

To explore the diagnostic performance of serum LPS and miR-142-3p, serum samples and medical records were collected from 40 patients with cirrhosis and 20 matched healthy controls. The baseline characteristics of the two groups are presented in **Table 1**. We found that serum LPS level was significantly higher and serum miR-142-3p level was significantly lower in cirrhosis patients than in control individuals (**Figure 6A**). We further examined the diagnostic capability of serum LPS and miR-142-3p levels among cirrhosis patients using ROC curve analysis. The AUCs for LPS and miR-142-3p were 0.872 (95% confidence interval [CI], 0.783-0.962; $P \leq 0.001$) and 0.662 (95% CI, 0.515-0.809; $P = 0.044$), respectively (**Figure**

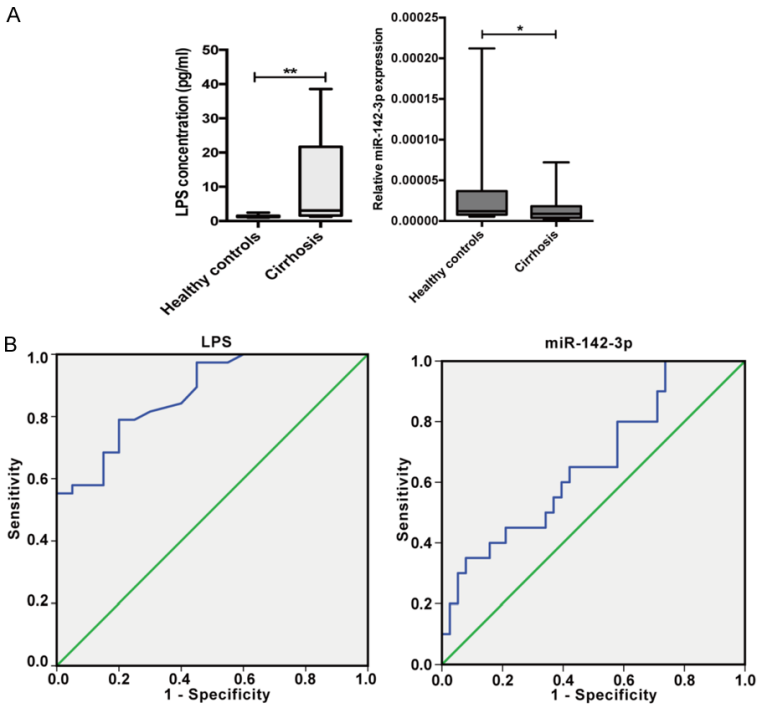

Figure 6. Diagnostic performance of serum LPS and miR-142-3p in patients with cirrhosis. A. ELISA was used to compare serum LPS and miR-142-3p levels between healthy controls (n = 20) and cirrhosis patients (n = 40). B. ROC curve analysis showed that LPS and miR-142-3p are potential biomarkers of cirrhosis. **, $P < 0.01$; *, $P < 0.05$.

6B). These results suggest that LPS and miR-142-3p are potential biomarkers of cirrhosis.

Discussion

As liver cirrhosis progresses, the circulation becomes increasingly hypercoagulable, hepatic veins outflow is impaired, and hypovolemia occurs. These pathological abnormalities lead to chronic hepatic congestion and local nutrient deficiency. From the perspective of energy expenditure, most liver cirrhosis patients are malnourished as a result of intake reduction, abnormal liver function, and insulin resistance [31-33]. Thus, the pattern of hemodynamics in cirrhosis resembles that in starvation [34]. In addition, a milestone of liver cirrhosis development could be microvascular ischemia. Microvascularity of liver sinusoids is presumed to underlie the clinical presentation of cirrhosis [1, 2]. As ischemia can induce autophagy and starvation is one ischemia condition [27], we employed starvation plus LPS treatment to mimic the pathological environment of cirrhosis. Our experiments demonstrated that lncRNA-TUG1 is upregulated in LSECs in a cirrhosis microenvironment and that TUG1 contributes to autophagy-mediated EndMT by binding with miR-142-3p and subsequently targeting ATG5, thereby relieving the repressive effect of miR-142-3p on ATG5.

In contrast to previous studies addressing the most-studied subpopulation of fibrogenic cells (i.e., activated hepatic stellate cells) of the liver during the profibrotic process, this study provides novel evidence of phenotypic and functional alterations of LSECs in a cirrhosis microenvironment consisting of starvation and a high concentration of LPS. TUG1 promotes hepatocellular carcinoma (HCC) and fibrotic diseases by accelerating the epithelial-mesenchymal transition in HCC cells and fibroblast transformation to myofibroblasts in endothelial cells in cardiac disorders [35, 36]. However, our results are novel in that they show lncRNA-TUG1 is enriched in LSECs. More importantly, this study is the first to explore the cirrhosis microenvironment-promoting effect of TUG1 in LSECs via autophagy-mediated EndMT.

Normal LSECs form a vascular type with a true basement membrane, whereas dedifferentiated LSECs contribute to the development of cirrhotic portal hypertension and microthrombosis. Therefore, it is plausible that LSECs contribute to the development of cirrhosis. Our study provides direct evidence that starvation and LPS treatment promote LSEC autophagy and EndMT *in vitro* and in an *in vivo* rat model of cirrhosis. Upregulation of autophagy has been considered as an adaptive response that protects LSECs from intracellular stresses [37], but it may not be sufficient to reverse the damages caused by cirrhosis. After increased autophagy, LSECs undergo a series of cellular transitions, such as loss of integrity and phenotype, which accelerate liver fibrogenesis. As EndMT is a critical process in fibrosis [38], a

better understanding of EndMT mechanism could help develop more effective therapeutic strategies for cirrhosis. The present study reveals that autophagy induced by starvation and LPS treatment is a crucial step in the EndMT of LSECs. Furthermore, TUG1, as a mediator of autophagy, is essential for inducing EndMT of LSECs in a cirrhosis microenvironment.

We found that TUG1 was highly expressed in LSECs, especially those subjected to starvation and LPS treatment. To elucidate the biological function of TUG1 in autophagy-mediated EndMT, we performed *in vitro* experiments showing that TUG1 knockdown inhibited the expression of genes related to autophagy and EndMT. Consistent with the increased level of TUG1, ATG5 was the most prominently increased autophagy-related gene in LPS-treated LSECs under starvation. Moreover, knockdown of TUG1 abolished the increase in ATG5 expression after LPS treatment, and inhibiting ATG5 attenuated autophagy and EndMT. These findings suggested that TUG1 contributes to autophagy and EndMT by targeting ATG5. Using the RNA FISH assay, we found that TUG1 was enriched in the cytoplasm and nucleus. Therefore, we assumed that cytoplasmic TUG1 might act as a ceRNA in the regulation of ATG5 expression. Using StarBase v2.0 and dual-luciferase reporter assay, we found that miR-142-3p regulated expression of TUG1 and ATG5. Many studies confirm that miR-142-3p serves as a tumor suppressor and cirrhosis blocker [39, 40]. However, its role in LSECs has not been examined. Furthermore, RIP with an antibody against Ago2 in LSECs confirmed that TUG1, ATG5 and miR-142-3p were recruited to an Ago2-related RISC, indicating that miR-142-3p plays an essential role in TUG1-mediated regulation of ATG5 expression in LSECs.

Considering the biological function of the ceRNA network in LSECs, we found that TUG1 negatively regulated the expression of miR-142-3p. Autophagy and EndMT were also decreased in LSECs after transfection with miRNA-142-3p mimics. These results indicate that the regulatory loop of TUG1-miR-142-3p-ATG5 maintains the transcriptional and posttranscriptional networks during the progression of cirrhosis. As serum LPS was upregulated whereas serum miR-142-3p was downregulated in cirrhosis patients, we conclude that serum LPS and miR-142-3p levels may inform the diagnosis and treatment of cirrhosis and that selectively targeting autophagy and EndMT in LSECs may be attractive approaches to preventing cirrhosis progression.

Our study has several limitations. First, the administration of 100 ng/mL or 1 μg/mL LPS treatment *in vitro and in vivo*, respectively, has been shown to promote fibrosis progression [41, 42]. However, whether starvation and 1 μg/mL LPS treatment physiologically reflects the mechanisms involved in liver cirrhosis requires verification by additional studies. Besides starvation, hypoxia, another ischemia condition, should also be considered because low oxygen stimulation affects autophagy [43]. Second, as LSECs change their phenotype to capillarization under pathological conditions, it may be better to experimentally study the relationship between autophagy/EndMT and capillarization and how such changes in LSECs affect liver fibrosis. Third, although we measured the co-localization of CD31 and α-SMA, more makers of EndMT are needed to verify our findings. Fourth, in addition to the diagnostic performance of LPS and miR-142-3p, their prognostic value deserves further consideration. LPS and miR-142-3p should also be compared to other well-known biomarkers of fibrosis. Finally, the possibility of preventing endothelial dysfunction by selectively targeting autophagy or EndMT in LSECs to interrupt the progression of liver cirrhosis requires further research.

In conclusion, our study shows that lnRNA-TUG1 mediates the LPS-induced promotion of autophagy-directed EndMT via sponging miR-142-3p and targeting ATG5 and suggests that miR-142-3p and LPS have considerable diagnostic and therapeutic potentials for cirrhosis.

Acknowledgements

This study was supported by the Innovation Fund of Science and Technology Commission of Shanghai Municipality (No. 15411950501, 15411950507 and 17140902700).

Disclosure of conflict of interest

None.

Abbreviations

ceRNAs, competing endogenous RNAs; EndMT, endothelial-mesenchymal transition; FISH, fluorescence in situ hybridization; RISC, RNA-induced silencing complexes; ROC, receiver-operating characteristic; TEM, transmission electron microscopy; VEGFA, vascular endothelial growth factor A.

Address correspondence to: Shi-Yao Chen, Department of Gastroenterology and Hepatology, Zhongshan Hospital, Fudan University, Shanghai 200032, P. R. China. Tel: +86-13601767310; E-mail: chen.shiyao@zs-hospital.sh.cn

References

[1] Mancuso A. The ischemic liver cirrhosis theory and its clinical implications. Med Hypotheses 2016; 94: 4-6.

[2] Mancuso A. Cirrhosis development probably arises from chronic microvascular ischemia. Med Hypotheses 2014; 82: 243-244.

[3] Seki E, De Minicis S, Osterreicher CH, Kluwe J, Osawa Y, Brenner DA and Schwabe RF. TLR4 enhances TGF-beta signaling and hepatic fibrosis. Nat Med 2007; 13: 1324-1332.

[4] Paik YH, Schwabe RF, Bataller R, Russo MP, Jobin C and Brenner DA. Toll-like receptor 4 mediates inflammatory signaling by bacterial lipopolysaccharide in human hepatic stellate cells. Hepatology 2003; 37: 1043-1055.

[5] Fouts DE, Torralba M, Nelson KE, Brenner DA and Schnabl B. Bacterial translocation and changes in the intestinal microbiome in mouse models of liver disease. J Hepatol 2012; 56: 1283-1292.

[6] Wanless IR, Liu JJ and Butany J. Role of thrombosis in the pathogenesis of congestive hepatic fibrosis (cardiac cirrhosis). Hepatology 1995; 21: 1232-1237.

[7] Tripodi A, Anstee QM, Sogaard KK, Primignani M and Valla DC. Hypercoagulability in cirrhosis: causes and consequences. J Thromb Haemost 2011; 9: 1713-1723.

[8] Ding BS, Cao Z, Lis R, Nolan DJ, Guo P, Simons M, Penfold ME, Shido K, Rabbany SY and Rafii S. Divergent angiocrine signals from vascular niche balance liver regeneration and fibrosis. Nature 2014; 505: 97-102.

[9] Wisse E, Braet F, Luo D, De Zanger R, Jans D, Crabbé E and Vermoesen A. Structure and function of sinusoidal lining cells in the liver. Toxicol Pathol 1996; 24: 100-111.

[10] McCuskey RS. Morphological mechanisms for regulating blood flow through hepatic sinusoids. Liver 2000; 20: 3-7.

[11] Poisson J, Lemoinne S, Boulanger C, Durand F, Moreau R, Valla D and Rautou PE. Liver sinusoidal endothelial cells: physiology and role in liver diseases. J Hepatol 2017; 66: 212-227.

[12] DeLeve LD. Liver sinusoidal endothelial cells in hepatic fibrosis. Hepatology 2015; 61: 1740-1746.

[13] Kaur J and Debnath J. Autophagy at the crossroads of catabolism and anabolism. Nat Rev Mol Cell Biol 2015; 16: 461-472.

[14] Chen W, Zhang Z, Yao Z, Wang L, Zhang F, Shao J, Chen A and Zheng S. Activation of autophagy is required for Oroxylin A to alleviate carbon tetrachloride-induced liver fibrosis and hepatic stellate cell activation. Int Immunopharmacol 2018; 56: 148-155.

[15] Thoen LF, Guimarães EL, Dollé L, Mannaerts I, Najimi M, Sokal E and van Grunsven LA. A role for autophagy during hepatic stellate cell activation. J Hepatol 2011; 55: 1353-1360.

[16] Deng J, Huang Q, Wang Y, Shen P, Guan F, Li J, Huang H and Shi C. Hypoxia-inducible factor-1alpha regulates autophagy to activate hepatic stellate cells. Biochem Biophys Res Commun 2014; 454: 328-334.

[17] Chen M, Liu J, Yang W and Ling W. Lipopolysaccharide mediates hepatic stellate cell activation by regulating autophagy and retinoic acid signaling. Autophagy 2017; 13: 1813-1827.

[18] Luo X, Wang D, Zhu X, Wang G, You Y, Ning Z, Li Y, Jin S, Huang Y, Hu Y, Chen T, Meng Y and Li X. Autophagic degradation of caveolin-1 promotes liver sinusoidal endothelial cells defenestration. Cell Death Dis 2018; 9: 576.

[19] Pardali E, Sanchez-Duffhues G, Gomez-Puerto MC and Ten Dijke P. TGF-β-induced endothelial-mesenchymal transition in fibrotic diseases. Int J Mol Sci 2017; 18.

[20] Suzuki T, Tada Y, Gladson S, Nishimura R, Shimomura I, Karasawa S, Tatsumi K and West J. Vildagliptin ameliorates pulmonary fibrosis in lipopolysaccharide-induced lung injury by inhibiting endothelial-to-mesenchymal transition. Respir Res 2017; 18: 177.

[21] Ribera J, Pauta M, Melgar-Lesmes P, Córdoba B, Bosch A, Calvo M, Rodrigo-Torres D, Sancho-Bru P, Mira A, Jiménez W and Morales-Ruiz M. A small population of liver endothelial cells undergoes endothelial-to-mesenchymal transition in response to chronic liver injury. Am J Physiol Gastrointest Liver Physiol 2017; 313: G492-G504.

[22] Young TL, Matsuda T and Cepko CL. The noncoding RNA taurine upregulated gene 1 is required for differentiation of the murine retina. Curr Biol 2005; 15: 501-512.

[23] Hu T, Fei Z, Su H, Xie R and Chen L. Polydatin inhibits proliferation and promotes apoptosis of doxorubicin-resistant osteosarcoma through

LncRNA TUG1 mediated suppression of Akt signaling. Toxicol Appl Pharmacol 2019; 371: 55-62.
[24] Yu G, Zhou H, Yao W, Meng L and Lang B. lncRNA TUG1 promotes cisplatin resistance by regulating CCND2 via epigenetically silencing miR-194-5p in bladder cancer. Mol Ther Nucleic Acids 2019; 16: 257-271.
[25] Han X, Hong Y and Zhang K. TUG1 is involved in liver fibrosis and activation of HSCs by regulating miR-29b. Biochem Biophys Res Commun 2018; 503: 1394-1400.
[26] Zhu Y, Feng Z, Jian Z and Xiao Y. Long noncoding RNA TUG1 promotes cardiac fibroblast transformation to myofibroblasts via miR-29c in chronic hypoxia. Mol Med Rep 2018; 18: 3451-3460.
[27] Gade TPF, Tucker E, Nakazawa MS, Hunt SJ, Wong W, Krock B, Weber CN, Nadolski GJ, Clark TWI, Soulen MC, Furth EE, Winkler JD, Amaravadi RK and Simon MC. Ischemia induces quiescence and autophagy dependence in hepatocellular carcinoma. Radiology 2017; 283: 702-710.
[28] Michalik KM, You X, Manavski Y, Doddaballapur A, Zörnig M, Braun T, John D, Ponomareva Y, Chen W, Uchida S, Boon RA and Dimmeler S. Long noncoding RNA MALAT1 regulates endothelial cell function and vessel growth. Circ Res 2014; 114: 1389-1397.
[29] Engreitz JM, Pandya-Jones A, McDonel P, Shishkin A, Sirokman K, Surka C, Kadri S, Xing J, Goren A, Lander ES, Plath K and Guttman M. The Xist lncRNA exploits three-dimensional genome architecture to spread across the X chromosome. Science 2013; 341: 1237973.
[30] Salmena L, Poliseno L, Tay Y, Kats L and Pandolfi PP. A ceRNA hypothesis: the Rosetta stone of a hidden RNA language? Cell 2011; 146: 353-358.
[31] Madden AM and Morgan MY. Resting energy expenditure should be measured in patients with cirrhosis, not predicted. Hepatology 1999; 30: 655-644.
[32] Caronia S, Taylor K, Pagliaro L, Carr C, Palazzo U, Petrik J, O'Rahilly S, Shore S, Tom BD and Alexander GJ. Further evidence for an association between non-insulin-dependent diabetes mellitus and chronic hepatitis C virus infection. Hepatology 1999; 30: 1059-1063.
[33] Holstein A, Hinze S, Thiessen E, Plaschke A and Egberts EH. Clinical implications of hepatogenous diabetes in liver cirrhosis. J Gastroenterol Hepatol 2002; 17: 677-681.
[34] Schneeweiss B, Graninger W, Ferenci P, Eichinger S, Grimm G, Schneider B, Laggner AN, Lenz K and Kleinberger G. Energy metabolism in patients with acute and chronic liver disease. Hepatology 1990; 11: 387-393.
[35] He C, Liu Z, Jin L, Zhang F, Peng X, Xiao Y, Wang X, Lyu Q and Cai X. lncRNA TUG1-mediated mir-142-3p downregulation contributes to metastasis and the epithelial-to-mesenchymal transition of hepatocellular carcinoma by targeting ZEB1. Cell Physiol Biochem 2018; 48: 1928-1941.
[36] Zhu Y, Feng Z, Jian Z and Xiao Y. Long noncoding RNA TUG1 promotes cardiac fibroblast transformation to myofibroblasts via miR-29c in chronic hypoxia. Mol Med Rep 2018; 18: 3451-3460.
[37] Ruart M, Chavarria L, Campreciós G, Suárez-Herrera N, Montironi C, Guixé-Muntet S, Bosch J, Friedman SL, Garcia-Pagán JC and Hernández-Gea V. Impaired endothelial autophagy promotes liver fibrosis by aggravating the oxidative stress response during acute liver injury. J Hepatol 2019; 70: 458-469.
[38] López-Novoa JM and Nieto MA. Inflammation and EMT: an alliance towards organ fibrosis and cancer progression. EMBO Mol Med 2009; 1: 303-314.
[39] Gao J, Wu N, Liu X, Xia Y, Chen Y, Li S and Deng Z. MicroRNA-142-3p inhibits cell proliferation and chemoresistance in ovarian cancer via targeting sirtuin 1. Exp Ther Med 2018; 15: 5205-5214.
[40] Yang X, Dan X, Men R, Ma L, Wen M, Peng Y and Yang L. MiR-142-3p blocks TGF-β-induced activation of hepatic stellate cells through targeting TGFβRI. Life Sci 2017; 187: 22-30.
[41] Chen M, Liu J, Yang W and Ling W. Lipopolysaccharide mediates hepatic stellate cell activation by regulating autophagy and retinoic acid signaling. Autophagy 2017; 13: 1813-1827.
[42] Yang Y, Wu XQ, Li WX, Huang HM, Li HD, Pan XY, Li XF, Huang C, Meng XM, Zhang L, Lv XW, Wang H and Li J. PSTPIP2 connects DNA methylation to macrophage polarization in CCL4-induced mouse model of hepatic fibrosis. Oncogene 2018; 37: 6119-6135.
[43] Abdul Rahim SA, Dirkse A, Oudin A, Schuster A, Bohler J, Barthelemy V, Muller A, Vallar L, Janji B, Golebiewska A and Niclou SP. Regulation of hypoxia-induced autophagy in glioblastoma involves ATG9A. Br J Cancer 2017; 117: 813-825.

Table S1. Primers for quantitative RT-PCR

Gene	Sequence
ATG7	Forward-5'-CTGTGGCATCTGCTGACCTC-3'
	Reverse-5'-AGGTCCGGTCTCTGGTTGAA-3'
ATG5	Forward-5'-TGGACAGTTGCACACACTAGGA-3'
	Reverse-5'-TCAGATGTTCACTCAGCCACTG-3'
Beclin1	Forward-5'-CACATCTGGCACAGTGGACA-3'
	Reverse-5'-GGAGCAGCAACACAGTCTGG-3'
P62	Forward-5'-TGGCCATGTCCTACGTGAAG-3'
	Reverse-5'-AGCCATCGCAGATCACATTG-3'
LC3B	Forward-5'-GGCGCTTACAGCTCAATGCT-3'
	Reverse-5'-GATTGGTGTGGAGACGCTGA-3'
GAPDH	Forward-5'-GGAGCGAGATCCCTCCAAAAT-3'
	Reverse-5'-GGCTGTTGTCATACTTCTCATGG-3'

Table S2. Lists of antibodies

Name	Cat No.	Methods	Supplier
anti-LC3B	3868	Western blots/Immunofluorescence	Cell Signaling Technology, Danvers, MA
anti-P62	88588	Western blots/immunohistochemistry	Cell Signaling Technology, Danvers, MA
Anti-CD31	Ab182981	Immunofluorescence	Abcam
Anti-CD31	Ab32457	Western blots	Abcam
Alexa Fluor 488 donkey anti-rat IgG (H+L)	A21206	Immunofluorescence	Life technologies
Alexa Fluor 594 donkey anti-rat IgG (H+L)	A21207	Immunofluorescence	Life technologies
Anti-α-SMA	Ab7817/BM0002	Western blots/Immunofluorescence	Abcam/Boster
Anti-VE-cadherin	2500S	Western blots	Cell Signaling Technology, Danvers, MA
anti-Atg5	12994	Western blots/immunohistochemistry	Cell Signaling Technology, Danvers, MA
anti-actin	AA128	Western blots	Beyotime biotechnology, China
anti-GAPDH	AG019	Western blots	Beyotime biotechnology, China

Table S3. TUG1 and ATG5 shared binding site for miR-142-3p

	miR-142-3p binding site
TUG1 3' UTR WT	5'-TGTATTAATATTTTACACTACC-3'
miR-142-3p	3'-AGGTATTTCATCCTTTGTGATGT-5'
TUG1 3' UTR Mut	5'-TGTCCTTCCTTTTTCATTCCTC-3'
ATG5 3' UTR WT	5'-CCTGTGTTCTTTACACACTACA-3'
miR-142-3p	3'-AGGTATTTCATCCTTTGTGATGT-5'
ATG5 3' UTR Mut	5'-CCTGTGTTCTTTACCACAGCAA-3'

Table S4. Primers for RNA immunoprecipitation (RIP) experiment

Gene	Primer Sequences (5' to 3')
Human GAPDH	F: CCATGACAACTTTGGTATCGTGGAA
	R: GGCCATCACGCCACAGTTTC
TUG1	F: TTTTTGAGAGCAGCATTGGA
	R: GTGACCTTCACGGGATCCTA
ATG5	F: AGAAGCTGTTTCGTCCTGTGG
	R: AGGTGTTTCCAACATTGGCTC
U6	F: CGCTTCGGCAGCACATATAC
	R: TTCACGAATTTGCGTGTCAT
miR-142-3p	RT primer: GTCGTATCCAGTGCAGGGTCCGAGGTATTCGCACTGGATACGACTCCATAAA F: GTCGTATCCAGTGCAGGG
	R: CGACGTGTAGTGTTTCCTA

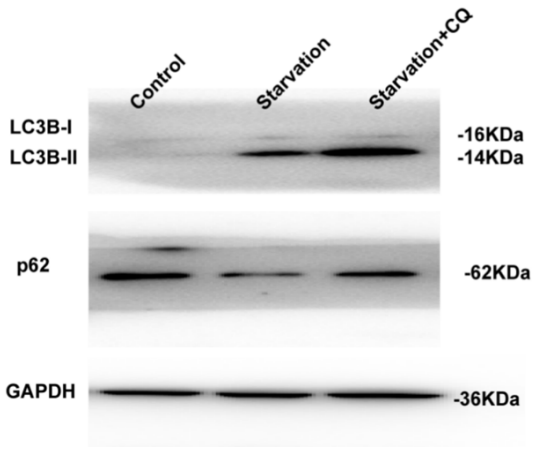

Figure S1. The original western images of **Figure 1D**.

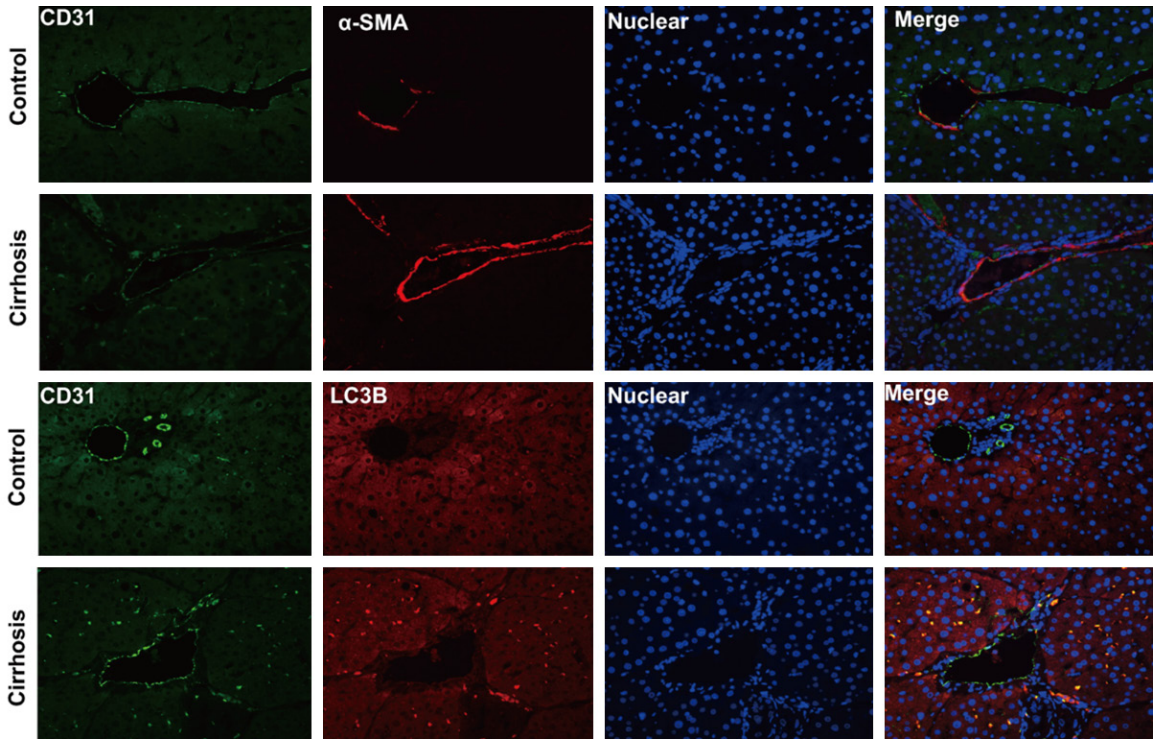

Figure S2. Immunofluorescent localization for CD31 counterstained with LC3B and α-SMA.

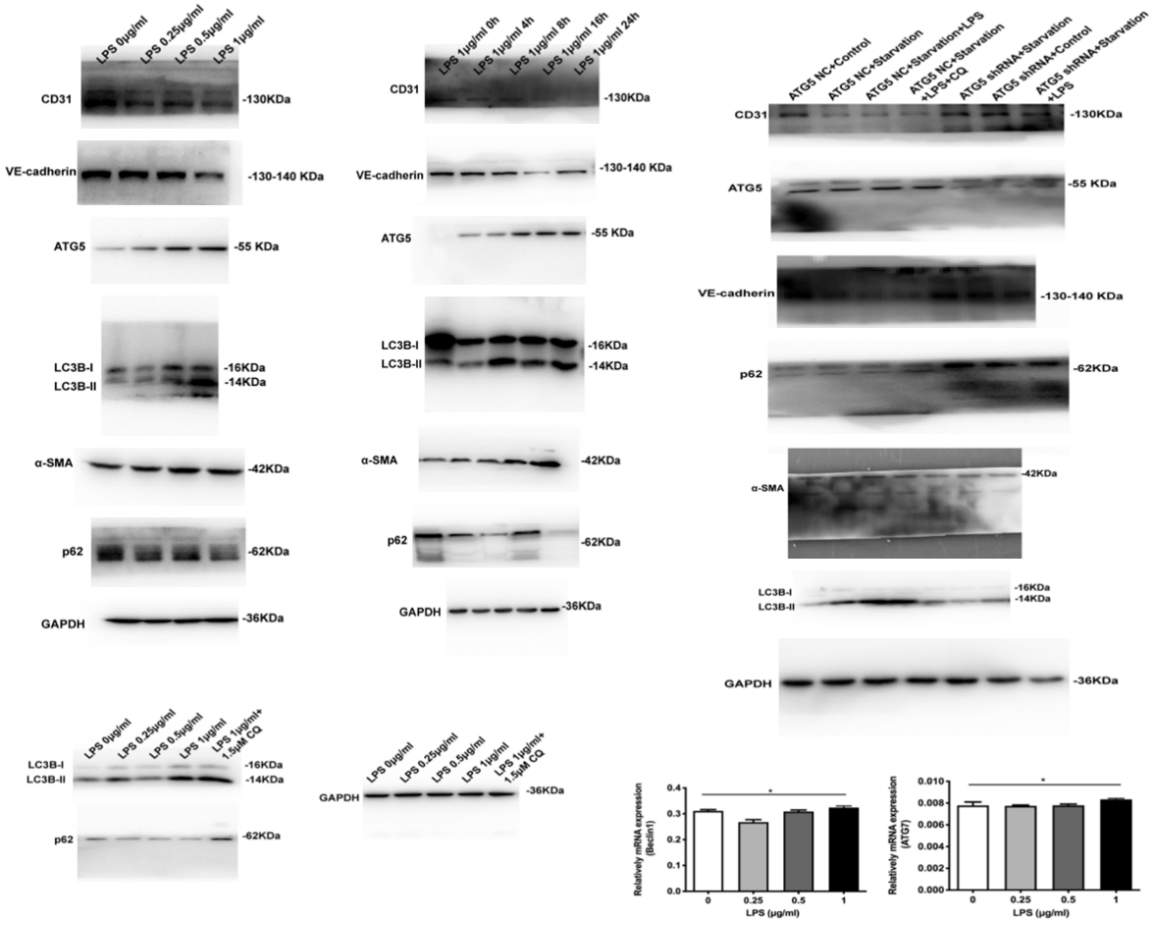

Figure S3. The original western images of **Figure 3** and the gene expression of ATG7 and Beclin1 in LSECs by LPS under starvation treatment.

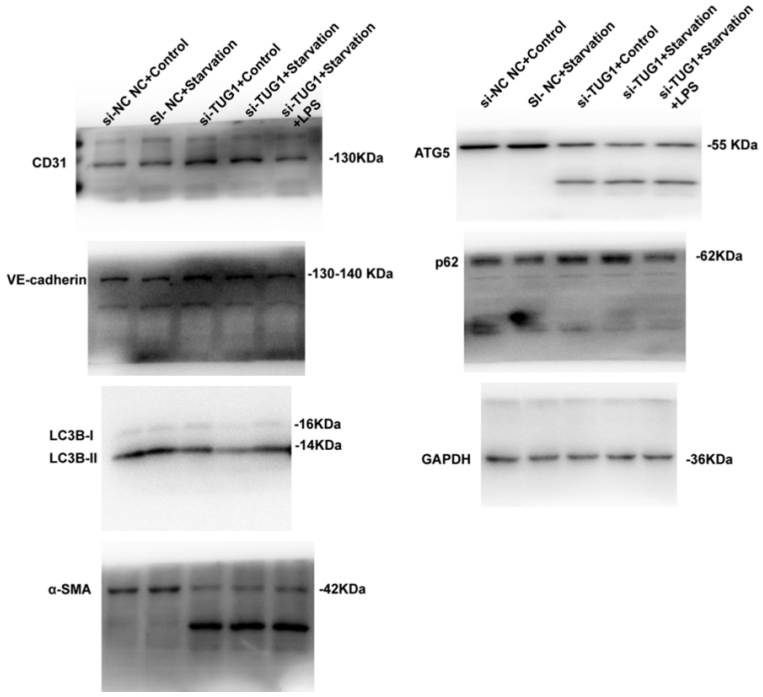

Figure S4. The original western images of **Figure 4**.

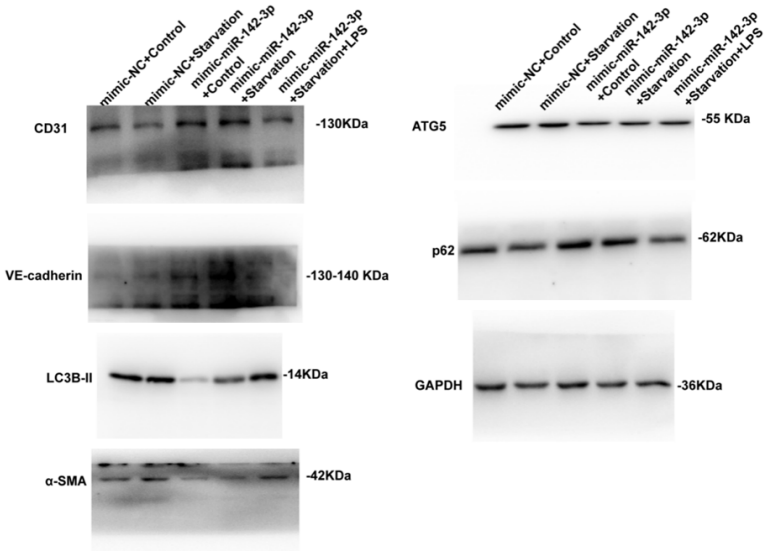

Figure S5. The original western images of **Figure 5**.